MDPI

New Control Strategy for Heating Portable Fuel Cell Power Systems for Energy-Efficient and Reliable Operation

Sebastian Zimprich, Diego Dávila-Portals, Sven Matthiesen * and Thomas Gwosch

Institute of Product Engineering, Karlsruhe Institute of Technology (KIT), 76131 Karlsruhe, Germany
* Correspondence: sven.matthiesen@kit.edu; Tel.: +49-721-60847156

Abstract: Using hydrogen fuel cells for power systems, temperature conditions are important for efficient and reliable operations, especially in low-temperature environments. A heating system with an electrical energy buffer is therefore required for reliable operation. There is a research gap in finding an appropriate control strategy regarding energy efficiency and reliable operations for different environmental conditions. This paper investigates heating strategies for the subfreezing start of a fuel cell for portable applications at an early development stage to enable frontloading in product engineering. The strategies were investigated by simulation and experiment. A prototype for such a system was built and tested for subfreezing start-ups and non-subfreezing start-ups. This was done by heating the fuel cell system with different control strategies to test their efficiency. It was found that operating strategies to heat up the fuel cell system can ensure a more reliable and energy-efficient operation. The heating strategy needs to be adjusted according to the ambient conditions, as this influences the required heating energy, efficiency, and reliable operation of the system. A differentiation in the control strategy between subfreezing and non-subfreezing temperatures is recommended due to reliability reasons.

Keywords: control strategies; environmental conditions; fuel cell; heating strategies; hydrogen; portable device; power system reliability; testing

1. Introduction

Hydrogen is a high-potential alternative fuel source, which can help reduce the emission of greenhouse gases into the atmosphere. Using renewable energies, this element can be obtained through the electrolysis of water. Hydrogen fuel cells (FC) can rely on different principles and are found in various sizes; however, all of them generate electrical energy via an electrochemical reaction [1]. Proton exchange membrane fuel cells (PEMFCs) have been developed for a wide span of power outputs, ranging from micro PEMFCs with 100 mW to applications requiring several kW [2–5].

Unlike in the automotive field, smaller portable applications currently on focus on the market-leading lithium-ion batteries and do not take fuel cell systems into account [6]. Considering the energy density of batteries nowadays (usually between 50 and 200 kWh/kg), the added weight from the additional battery units poses a problem for most portable applications [7]. A comparison of the energy and power density for different types of energy storage systems was shown by Julien et al. [7]. Therefore, the search for lighter energy carriers could significantly impact the technology behind battery-powered machines. A weight reduction in the energy carriers could be realized by replacing traditional batteries with PEMFCs.

A proton exchange membrane fuel cell (PEMFC) requires a constant supply of fuel (i.e., hydrogen). A suitable option for this purpose is a metal hydride tank, which stores hydrogen at a low-pressure level compared to pressure tanks, in a dissolved state into metal particles. These may release or absorb the hydrogen gas depending on the pressure inside the tank. With respect to its discharge behavior, the tank presents a constant pressure

for a wide range of hydrogen supply. Hence, a metal hydride tank shows an optimal behavior for the supply of hydrogen to smaller and portable PEMFCs, such as the tanks lower pressure level due to safety reasons.

Currently, there are mechanisms that demonstrate better energy and power density values when compared to lithium-ion batteries, which are the industry standard for most applications. This indicates that lithium-ion batteries could be substituted by alternative technologies, such as fuel cell systems. Especially for tasks with increased energy demands due to longer utilization periods, PEMFCs would be advantageous [8]. The key characteristics highlighting PEMFCs' superior functionality for portable applications are their lack of reliance on the power grid, their reliability, and their increased energy density when compared to batteries. PEMFC systems as energy carriers can have an energy density of about 850 Wh/kg. The benefits of PEMFC systems, when compared to classical battery systems, increase with an increasing operation time [7–9].

A portable fuel cells performance is challenged when operating at low (<0 °C) and increased ambient temperatures (>40 °C). Current and power drop with lower temperatures, which leads to a decrease in efficiency [10–13]. With every succeeding subfreezing start-up, the current density can drop further due to permanent damage in the membrane caused by ice formations [1,12]. By electrically heating up a PEMFC stack, it will achieve higher temperatures significantly faster when compared to passive heating caused by its own heat losses [14]. Therefore, the subfreezing start-up of PEMFCs sets a barrier towards its further commercialization [15]. This characteristic trait is found to negatively affect many portable devices. Potential portable applications can be power generators, drone applications, or power tools. Unfortunately, in everyday environments, subfreezing temperatures are fairly common and at times unavoidable. As a result, it is vital to look for appropriate solutions allowing devices powered by a PEMFC to function under subfreezing temperatures.

Due to the weight and size constraints of portable machinery, the available space to construct a solution is quite limited. Different strategies have been proposed to enable the subfreezing start-up of a PEMFC [16–18]. There are two common methods used for the subfreezing start-up of a PEMFC. The first method includes purging the device prior to shutting it down and humidifying it before start-up. This extracts the water inside the membrane, which results from the operation of the PEMFC. The second method heats up the device before start-up in order to reach temperatures above the freezing point of water [12–15,19,20]. However, the first method, which purges and humidifies the device, would require an additional subsystem. As this would require an adequate amount of space and add weight to the system, it would undermine the portable characteristics of the device. In addition, at subfreezing temperatures, this alone cannot reliably prevent the formation of ice, as there is no way to determine whether all water has been removed from the cell.

Many other patents and invention disclosures have solved the subfreezing start-up problem by circulating a previously heated liquid around the FC. This, however, is not suitable for portable applications, as this contradicts the weight and size restrictions [21–25]. By reversing the polarity of the cell, a reverse current flow through the PEMFC generates heat. This may cause degradation within the cell after several uses [15,26,27]. Therefore, this solution is not ideal for the subfreezing start-up of a PEMFC despite its simplicity as well as its low weight and volume.

Inserting a higher amount of hydrogen into the anode causes an exothermic reaction that heats the cathode [28]. Another possibility is to keep the stack temperature in a specified range by using electrical heaters, in turn preventing ice formations [29,30]. Keeping the stack temperature in a specified range over a long period of time would require a great deal of energy, which is not suitable for portable applications. More simplistic solutions have been suggested where the stack has electrical heaters that raise the temperature only prior to the actual start-up [31,32]. Given that this system's functionality adds minimal weight and volume to the device, it may be a suitable solution to heat the small PEMFCs during a subfreezing start-up. In addition, the hydrogen supply is highly dependent on the

temperature and is critical for the PEMFCs operation. Therefore, the thermal management strategy for the hydrogen tank has to be considered in portable applications [9].

Due to weight and size constraints of portable machinery, only a limited amount of energy can be used for the heating. The used heating strategy needs to provide enough heating power to achieve this heating process for the PEMFC. As a result, the energy storage has to provide enough energy for the strategy. The control strategy has to take into account the strict weight and size constraints that a portable device imposes. Therefore, the influence of ambient temperature on the heating strategy is especially relevant in portable applications. The ambient conditions influence the required energy, reliability, as well as efficiency of the PEMFC system; however, its effects under portable constraints are currently unknown.

A tradeoff between the heating strategies and portable constraints has to be considered to ensure a reliable operation. The goal of this study is therefore to investigate and validate heating strategies for environments in which portable FC are subjected to subfreezing temperatures.

2. Materials and Methods

In the following chapter, the experimental procedure is presented. This includes the control strategies and modeling, the simulations, the individual experiments, as well as the procedures used to collect the experimental data.

The prototype used for this study is a modified portable cordless screwdriver that is based on a Festool PDC 18/4. It was modified to function using a 20 W PEMFC stack and a small energy buffer. The energy buffer has a maximum power output of 900 W and a capacity of 43.3 kJ. This setup is used for all experiments conducted in this study as well as for the necessary parametrizations needed for the simulation models [33]. This prototype is presented in detail in a preliminary study [33].

2.1. Control Strategy and Study Design

Prior to start-up, when warming up the PEMFC at subfreezing ambient temperatures, potential ice formations in the cathode melts before the internal reaction begins. As a result, damage to the membrane can be avoided. This may also influence the power output and efficiency of the cell. Through the use of different sensors, temperatures and ice formations could be directly measured and/or detected within the cell. Unfortunately, due to the lack of space within the PEMFC membrane, these sensors cannot be included in the design. This leads to uncertainties, which cannot be solved by simulation or component tests. In order to investigate these uncertainties, testing the overall system is necessary.

Therefore, the ambient temperature (T_a) as the test case (TC) and the temperature at which the heater is turned off (T_{HO}) as the control strategy (CS) are investigated in this study. The ambient temperature T_a is varied in two test cases. Test case one (TC1) is a non-subfreezing start-up with $T_a = 5\,°C$. Test case two (TC2) is a subfreezing start-up with $T_a = -3\,°C$.

The heating is performed until a certain measured temperature in the PEMFC is reached. When the temperature is reached the first time, the heater is turned off. By varying the temperature at which the heater is turned off (T_{HO}), the effect of the control strategies on the power output, efficiency, and reliability can be investigated. The PEMFC in this study has a nominal temperature is 50 °C, and this temperature was used for control strategy one (CS1) as T_{HO}. Control strategy two (CS2) has a temperature T_{HO} just over the freezing point of water, with $T_{HO} = 5\,°C$. This demonstrates whether the heating strategy is enough for a safe subfreezing start-up as well as how much energy is required for the different strategies to function properly. The four possible combinations of TC and CS are given in Table 1. The four combinations are tested in this study by experiment and simulation.

Table 1. Control strategy study design with the four tests as combination of CS and TC.

		Ambient Temperature T_a	
		TC1: T_a = 5 °C	TC2: T_a = −3 °C
Turn-off temperature T_{HO} in the control strategy	CS1: T_{HO} = 5 °C	Test 1/1	Test 1/2
	CS2: T_{HO} = 50 °C	Test 2/1	Test 2/2

The heaters controller, specifically for the hydrogen tank, may deliver the same output for all experiments carried out at temperatures 15 °C and 25 °C. This is justified by the steady hydrogen flow maintained throughout these tests. This temperature range was obtained from the study conducted by Kyoung et al. It allows the pressure output of the hydrogen tank to lie within a range that allows for normal operation of the PEMFC [9].

The control strategy is made up of three parallel paths. It starts when the device is turned on. On the left side of Figure 1, the state flow diagram for the hydrogen supply control strategy to the PEMFC membrane is shown. Here, the valve is only opened when the temperature of the FC is above 5 °C. When the temperature in the tests decreases and drops below 5 °C, the valve is closed to prevent permanent damage to the membrane. In the middle path, the control strategy for the FC heater is shown. The heating starts when the FC temperature is below T_{HO}. Once T_{HO} is reached for the first time, the start-up heating is completed, and the heater is turned off.
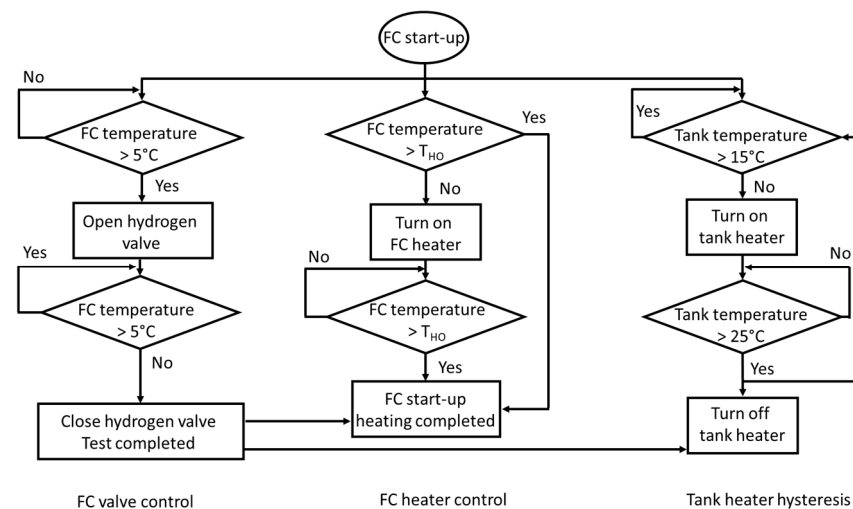
Figure 1. PEMFC's systems control strategy in this study.

The right path in Figure 1 shows the hysteresis controller for the metal hydride tank heater. The hysteresis controller keeps the tank temperature in a range between 15 °C and 25 °C. The tank heater, as well as the FC heater, are stopped by the left part if the FCs temperature drops below 5 °C, as the tests are completed there. The complete control strategy is shown in Figure 1.

2.2. Mathematical Simulation Model

The model design is based on the physical components of the cordless screwdriver. Figure 2 shows the structure of the proposed system, as well as the interaction between individual components. This design focuses on the system's thermal behavior as well as the necessary components needed to apply the heating control strategy. The grey-colored blocks were not considered in the model. Although they belong to the power supply subsystem, they were out of the scope of this study.
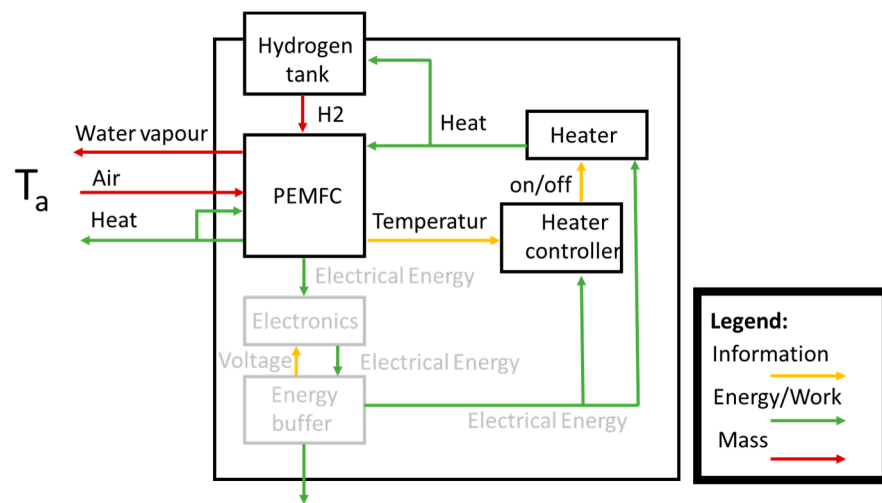
Figure 2. Functional structure of the fuel-cell powered screwdriver system.

The ambient temperature T_a is considered the environmental parameter in this model. It is assumed that similar parameters have little to no influence on the system's behavior. The thermal model used in this study takes two subsystems into account: the PEMFC and the hydrogen tank. Figure 3 shows the thermal circuit for these subsystems. Here, the thermal masses are represented by ellipses, while heat transfers are represented by rectangles. The heaters are represented as triangles. The PEMFC and the hydrogen tank are thermally isolated from each other. The environment is assumed to be an ideal temperature source with constant temperature T_a.
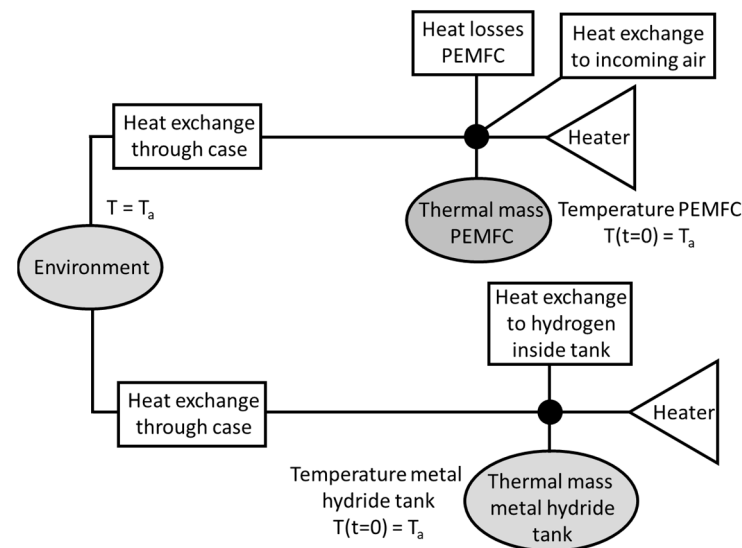

Figure 3. Thermal model of the PEMFC system.

Both the PEMFC and hydrogen storage are modeled as thermal masses with the starting temperature T_a. The thermal mass of the metal hydride tank is measured at 275 J/K. The thermal mass of the PEMFC is modelled with 81 J/K. Heat conduction, convection, and radiation are considered as well as heat exchange with fluids. The effect of the air between the hydrogen tank and the case is negligible. The PEMFCs heater has a heating power of 70 W, while the metal hydride tanks heater has a heating power of 30 W.

$$\dot{Q}_{A \rightarrow B} = \lambda_{A \rightarrow B} * (T_B(t) - T_A(t)) = \sum \dot{Q}_{cond} + \sum \dot{Q}_{conv} + \sum \dot{Q}_{rad} \tag{1}$$

In our model, the heat exchanged between two points is described as the product of the heat conductivity $\lambda_{A \to B}$ and the difference in temperature T between them. As shown in Equation (1), both variables were in this case time-dependent. Alternatively, this can also be expressed as the summation of all heat exchange mechanisms applied to the different points of the heat transfer chain. All three heat exchange mechanisms were considered for the five heat transfer paths, represented as rectangles in Figure 3. For the different heat transfer mechanisms, temperature-dependent coefficients were calculated. These were assumed to be constant throughout the simulation. The single coefficients were not validated by experiment, as this would require a complex experiment for each coefficient [34]. The balance of absorbed/released energy by the reaction inside the PEMFC was calculated using the gravimetric flows $\dot{m}$ for both the incoming reactants and the outgoing products. The corresponding specific enthalpy values were calculated h_x, using the gas's temperatures.

An electrical model of the PEMFC was implemented since its electrical output has the most significant influence on the power supply subsystem. It was modeled as a Thevenin's equivalent circuit with a diode, as proposed by Njoya et al. [35]. The PEMFC's losses as well as the heating power of the heaters were calculated from its electrical model and the heaters, respectively. Equation (2) displays the mathematical definition of its output voltage V. This depends on the open circuit voltage V_{OC}, the number of cells in the stack N, the Tafel slope A of the voltage-current curve, the exchange current i_O, and its current i_{FC} respectively, as well as the response time T_d. Its open-circuit voltage V_{OC} was calculated, as shown in Equations (3), as the product of the voltage constant at nominal operation K_C and the Nernst voltage E_n. The exchange current i_O, shown in Equation (4), is a function of the Boltzmann's constant k, the partial pressures of hydrogen p_{H2} and oxygen p_{O2}, the ideal gas constant R, the Planck's constant h, the activation energy barrier ΔG, and the temperature of operation T. Finally, Equation (5) shows that the Tafel slope A is a function of the ideal gas constant R, the temperature T, and the charge transfer coefficient α.

$$V = V_{OC} - N * A * ln\left(\frac{i_{fc}}{i_0}\right) * \frac{1}{s * T_d/3 + 1} \tag{2}$$

$$V_{OC} = K_C * E_n \tag{3}$$

$$i_0 = \frac{2 * 96485 \left[\frac{A * s}{mol}\right] * k * \left(p_{H_2} + p_{O_2}\right)}{R * h} * e^{-\frac{\Delta G}{R * T}} \tag{4}$$

$$A = \frac{R * T}{2 * \alpha * 96485 \left[\frac{A * s}{mol}\right]} \tag{5}$$

The used 20 W PEMFC stack at nominal operation delivers 7.8 V and 2.6 A. The nominal operating temperature range lies at 55 °C and the nominal ambient temperature range between 5 °C and 30 °C. This of course reinforces the argument for using heating strategies for a subfreezing start-up. The nominal hydrogen pressure lies between 0.45 and 0.55 bar depending on the storage temperature. This shows that the temperature of the hydrogen storage needs to be managed as well since it has an important impact on its pressure. It is worth noting that this PEMFC's nominal efficiency is 40%.

The PEMFC had a power output depending on its temperature and electrical load. This demonstrates the importance of implementing heating strategies in order to generate the highest power output from the cell [36]. The implemented model for the metal hydride hydrogen storage for the adsorption pressure of the metal hydride is based on Kyoung et al. [9]. Equation (6) shows the outgoing flow from the tank Q_{out} in relation to the opening

cross-section A_{out}, the difference of pressure between the tank and the environment Δp, and the density of the gas ρ.

$$Q_{out} = A_{out} * \sqrt{2 * \frac{\Delta p}{\rho}} \tag{6}$$

The flow between devices was transported through plastic tubes and was assumed to be adiabatic. The amount of heat absorbed by the incoming gases from the PEMFC's membrane was negligible for determining its temperature.

Table 2 shows the list of variables that were considered in the above-mentioned simulation. These variables were considered in the experiments as well.

Table 2. Observed variables in this study.

Controlled Variables	Measured Dependent Variables
Initial temperature of the PEMFC, i.e., ambient temperature	Average mass flow of hydrogen
Start and shutdown temperature of the PEMFC's heater	PEMFC's temperature
Start and shutdown temperature of the hydrogen storage's heater	Hydrogen storage's temperature
On/off states of heaters for the PEMFC and the hydrogen storage	PEMFC's voltage and current
On/off state of hydrogen valve	Voltage source's current

The simulation model considered all relevant subsystems for the investigated thermal behavior. It also included some simplifications along the entire system that left out variables that had a negligible impact on the studied behavior. The model was implemented into Matlab Simulink. The goal of these simulations was to virtually test the required heating energy for the heaters of the PEMFC and hydrogen tank. The PEMFC's temperature was evaluated in these simulations. These could then be related back to heating strategies aiding the subfreezing start-up of a PEMFC-powered portable device. This is achieved by using the XiL-approach (X-in-the-Lopp, Software-in-the-Loop SiL, Hardware-in-the-Loop HiL). This method is carried out by taking a component of a sub-system (HiL) or the algorithm of [37] the heating strategy (SiL) and repeatedly testing its influence on the entire system, while slight changes are made with every iteration.

The simulation was carried out with the four tests listed in Table 1. After that, experiments were carried out to take the PEMFC's efficiency and therefore the reliability of the system into account. The experimental setup is further explained in the following sub-section.

2.3. Test Bench for Experimental Investigation

Figure 4a shows the experimental setup. The prototype was held in place inside an enclosure where the ambient temperature T_a was set to the desired value. The refrigeration unit Huber Unistat 425 was used to cool the air inside [38]. The enclosure was made of 3 mm Plexiglas. The heat exchanger and ventilator were placed on top of the experiments enclosure. A near constant temperature within the enclosure replicated the ambient conditions typically found in real environmental conditions. The necessary sensors and controllers for the tests were attached to the prototype, as shown in Figure 4b.

Figure 5 shows the scheme of the experimental design. The sensors given in Table 3, heaters, and valve were attached to the prototype and connected to their respective control modules. This had a parallel bus interface that enabled the connection to the processor module. The processor module was connected via an Ethernet cable to the computer.
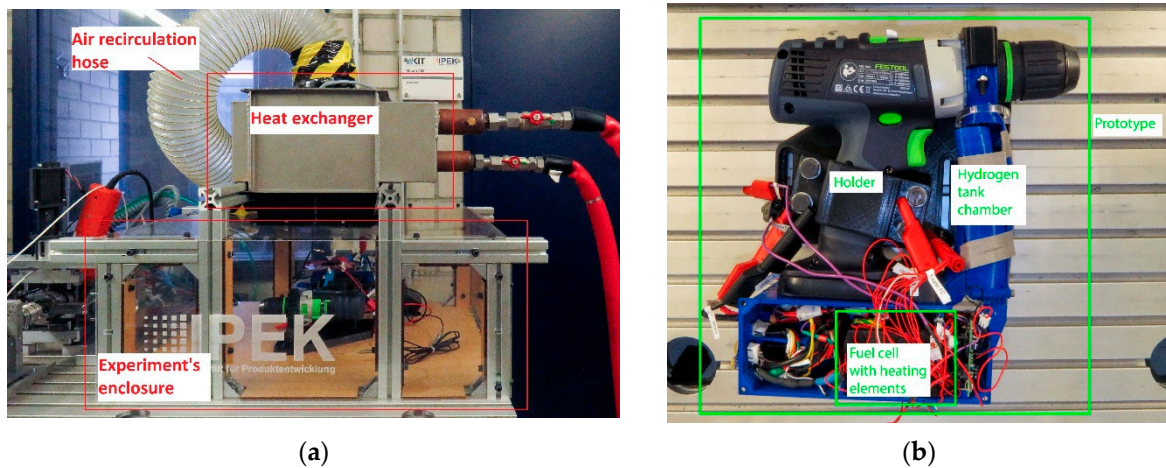
Figure 4. (**a**) Experimental setup with cooling system; (**b**) prototype used with PEMFC heaters.
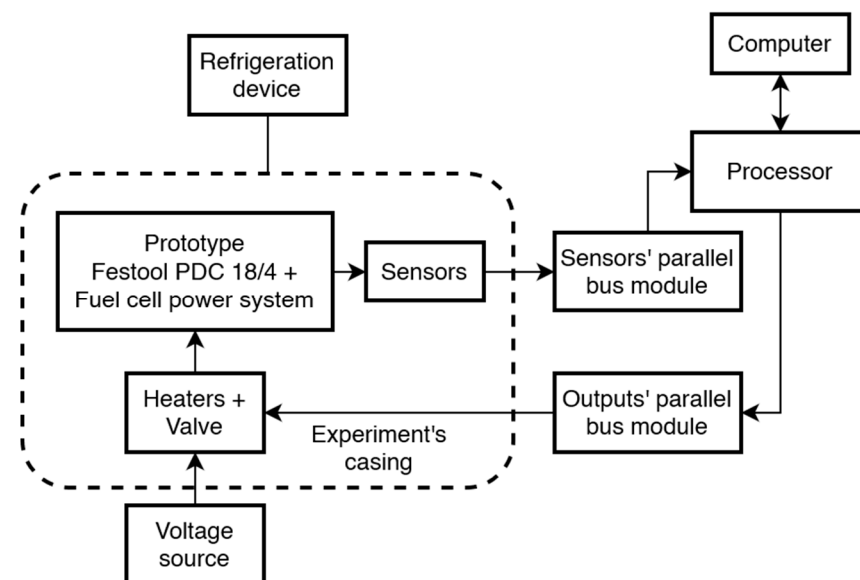

Figure 5. Scheme of the experimental design.

Table 3. Sensors used and variables measured in the experiments.

Sensor/Measuring Device	Variable
Scale	Average Hydrogen consumption
Thermocouple type J	PEMFC's temperature
Thermocouple type J	Hydrogen storage's temperature
Voltage Transducer type LV 25-P	PEMFC's voltage
Current Transducer type CASR	PEMFC's current
Voltage Transducer type LV 25-P	Battery's voltage
Current Transducer type CASR	Battery's current

A ADwin-Pro II was used as a processor for control and data acquisition [39]. The control algorithm was coded, compiled, and monitored using Matlab Simulink. In order to heat up the PEMFC and the hydrogen storage, heating foils were attached to them. Due to the limited space on the PEMFC and the hydrogen tank, multiple 10 W polyimide heating films were used for this study. The required heating energy for the control strategies is unknown. Therefore the heating foils were powered by a supply module EA PS9040-20T. It

was set to provide a constant direct current voltage of 18 V, which represented the nominal voltage of the battery that was originally used in this prototype. The PEMFC's output was connected to a resistor with a resistance of 3 Ω, which simulated the ideal load for its nominal working point (i.e., 7.8 V@2.6 A). PEMFC's voltage and current are measured to rate the system's power output. The mean efficiency is calculated by dividing the total power output of the PEMFC by the chemical energy of the hydrogen used.

The required start-up time and heating energy is evaluated for simulation and experiment in the four tests. The start-up is completed when the fuel cell heater and the metal hydride tank heater are both shut off. At this point, the desired temperature T_{HO} is reached, and the hydride tank is in the temperature window between 15 °C and 25 °C. The tank temperature can drop below 15 °C afterward as hydrogen is released to the PEMFC. Therefore, further heating energy is used to keep the metal hydride tank in the desired temperature window between 15 °C and 25 °C. Since the start-up is already completed, this energy is therefore not included in the evaluation of the start-up energy. By comparing the required heating time and energy between experiment and simulation, the validity of the simulation is evaluated. For this, the relative error between simulation and experiment is calculated for the start-up time and heating energy.

3. Results

The following sections presents the results obtained for the conducted simulations and experimental investigations. Simulations were conducted to investigate the effect the control strategy and test cases have on the thermal behavior and required heating energy. Taking the reliable operation and efficiency into account, the experimental investigations were carried out to validate the simulations.

3.1. Simulation Results

The simulations of the PEMFC power supply system were performed, using the proposed heating strategies, for the four different test cases. The ambient temperature (i.e., the initial temperature) T_a of the system and the temperature at which the heating strategies shut down the heaters T_{HO} were varied in these simulations. Figure 6 displays the necessary heating energy over time for the different simulations that were conducted.
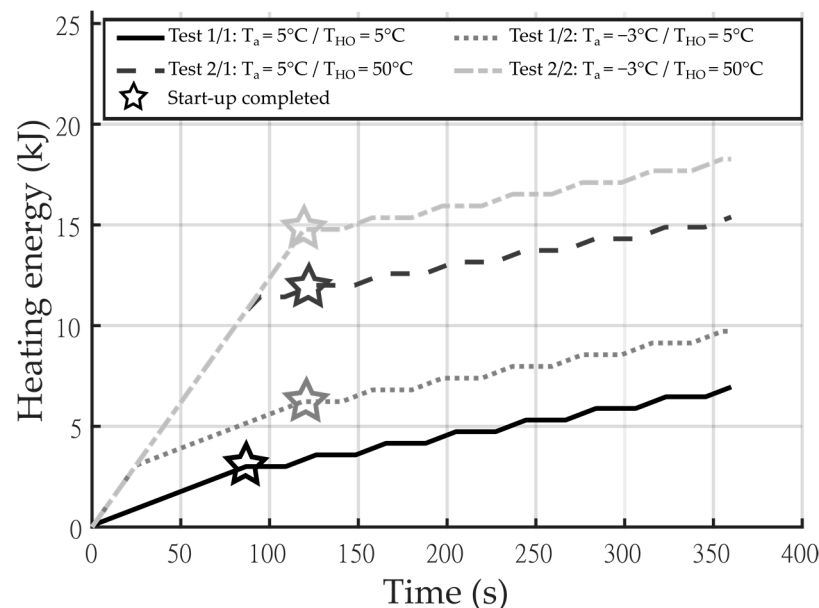

Figure 6. Heating energy required for the heaters of the PEMFC and hydrogen tank.

The tests showed a steep slope when both heaters (of the PEMFC and the hydrogen tank) were turned on. A smaller slope was observed when only the heater for the hydrogen tank was heating and no slope when both heaters were turned off.

The simulations with a lower ambient temperature T_a required more heating energy compared to those with a higher ambient temperature. This can be seen in Figure 6, when looking at the steeper slope for test 1/2, test 2/2, and test 2/1 at the beginning of the simulation compared to test 1/1. The steeper slope in the three tests is due to the fact that the fuel cell heater was switched on. In the other tests, only the tank heater was turned on at the start.

After some time, the slope decreased when the fuel cell heater was turned off, showing the hysteresis of the hydrogen tank's heater for the selected temperature range. More heating energy was required when the heating strategy shut down the heater of the PEMFC at higher temperatures T_{HO}. In the simulation, T_{HO} had a larger effect on the required heating energy than T_a.

3.2. Experimental Results

With the selected heating strategies and the different tests carried out (see Table 1), the conducted experiments demonstrated how control strategies in a portable system behave with respect to its components. Figure 7a shows the development of the PEMFC's average temperature over time. Test 1/1, starting at T_a = 5 °C, showed only a slow temperature rise during its operation, as T_{HO} was also set to 5 °C, and therefore, no energy was used to heat the PEMFC. However, energy was used to heat the metal hydride tank to ensure a steady hydrogen flow. The lower the starting temperature, the longer it took to reach higher temperatures. Changing the ambient temperature T_a to −3 °C in test 1/2 and shutting off the heater at T_{HO} = 5 °C showed a drop in the PEMFC's temperature. A temperature above 5 °C at a subfreezing ambient temperature could not be maintained without external heating, as the temperature dropped after turning off the heater. Test 2/1 and test 2/2 had a tendency to reach a stable operating temperature after shutting down the PEMFC's heaters. The longest time that the heating strategies took to reach their shutdown temperature was 270 s, which occurred in test 2/2. After the temperature T_{HO} is reached, the PEMFC heater shuts off. If the temperature drops, afterward, the heating is not restarted by the control strategy; instead, as in the study, the start-up behavior is investigated. However, the control strategy prevents a PEMFC operation below 5°C to prevent permanent damage to the membrane.
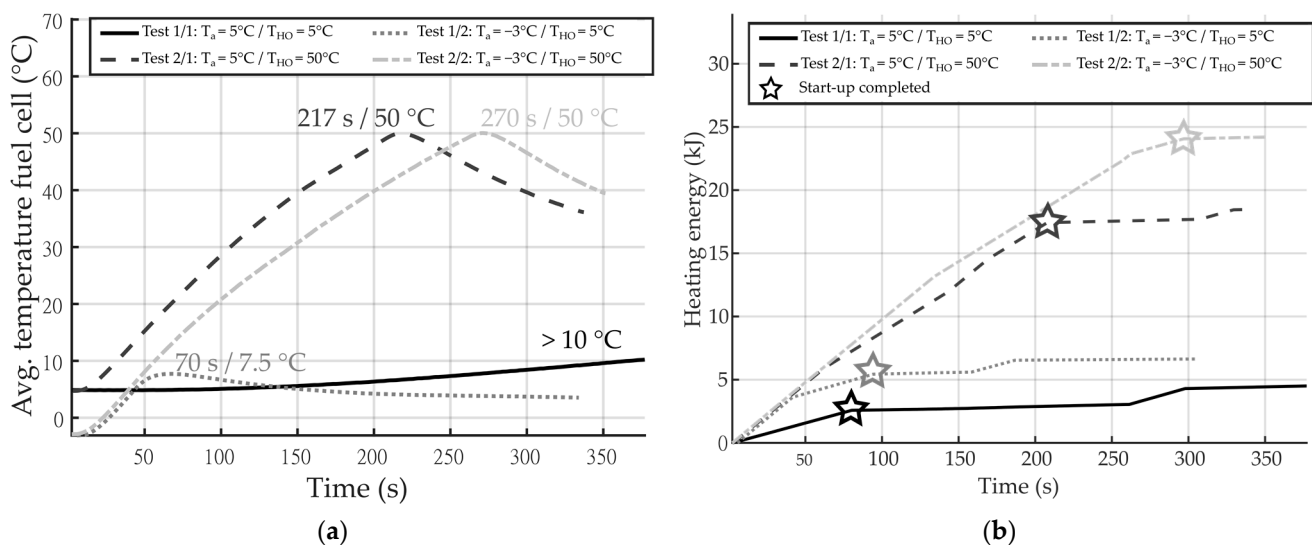

Figure 7. (**a**) PEMFC's average temperature development over time for different heating strategies; (**b**) heating energy of the PEMFC and hydrogen tank required in the four tests.

Figure 7b displays the heating energy required for the different tests. The control strategies that had higher shut-off temperatures T_{HO} for the heater, required more energy compared to those where the shut-off temperature was lower. The same applied for the experiments where the ambient temperature T_a was lower in comparison with those where it was higher. After reaching the temperature T_{HO}, when the PEMFC's heater shuts off, the energy curve's slope decreased, as only the hydrogen tank was heated to stay in a temperature range from 15 °C to 25 °C. In total, the maximum energy required throughout the tests was in test 2/2, with approximately 25 kJ. It is worth noting that test 2/2 had the lowest ambient temperature and highest shut-off temperature.

Table 4 compares the required start-up time and energy for the four tests in simulation and experiment. Test 1/1 had the smallest relative model error between simulation and experiment for the start-up time (8.0%) The smallest relative model error between simulation and experiment for the start-up heating energy (14.6%) was derived from test 1/2. The largest relative model error for the start-up time was shown in test 2/1 (-87.7%). The largest relative model error for the start-up energy was shown in test 2/2 (-38.6%). The negative relative model error indicates a larger value in the experiment compared to the simulation.

Table 4. Required start-up heating time and energy in simulation and experiment.

Test	Simulation Start-Up Time and Energy	Experiment Start-Up Time and Energy	Relative Model Error
1/1	86.8 s/3.0 kJ	80.3 s/2.6 kJ	8.0%/16.5%
1/2	118.6 s/6.2 kJ	94.2 s/5.4 kJ	-54.4%/14.6%
2/1	94.7 s/11.4 kJ	207.9 s/17.4 kJ	-87.7%/-34.4%
2/2	119.7 s/14.8 kJ	296.7 s/24.1 kJ	-59.6%/-38.6%

Figure 8a shows the required heating power. Since the heater of the hydrogen tank consumed approx. 30 W, and the heater of the PEMFC consumed approx. 70 W, the required power for heating the PEMFC and the power for heating the hydrogen tank can be separated. For all tests, energy is used to heat the hydrogen tank after the PEMFC is fully heated up. In test 1/1, the energy is only used to heat the hydrogen tank.
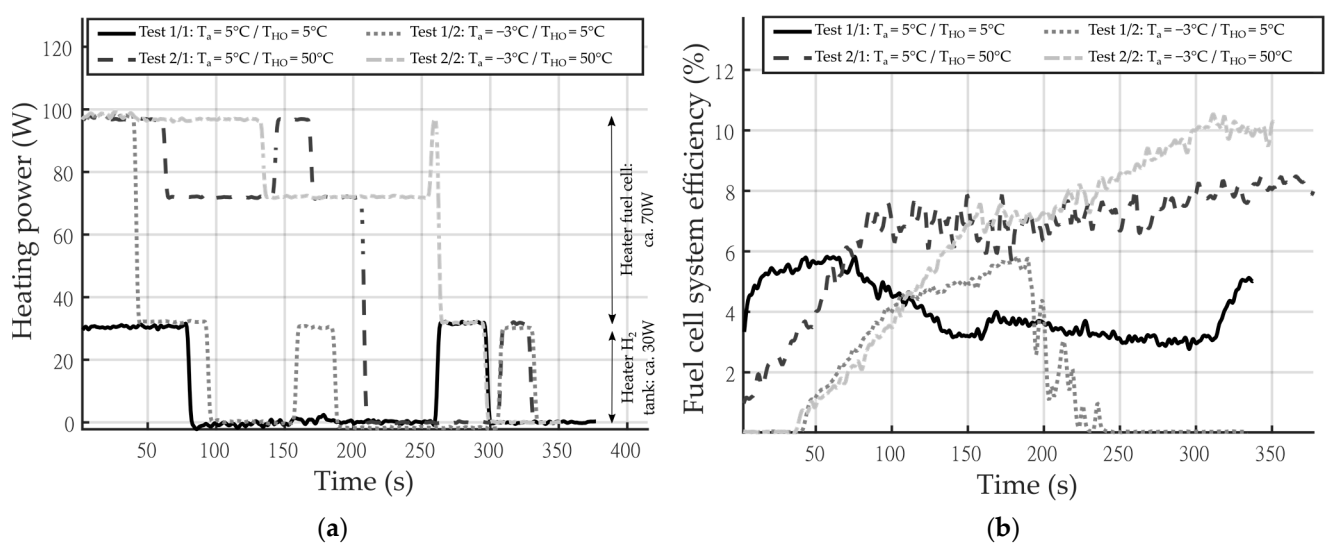

Figure 8. (**a**) Power consumption over time of the four for different tests; (**b**) PEMFC's efficiency over time for the four different tests.

Figure 8b shows the efficiency of the PEMFC system. Tests in which the system was heated up to T_{HO} = 50 °C reached a higher mean efficiency (test 2/1 = 6.55%, test 2/2 = 6.69%)

compared to the tests with heating up to $T_{HO} = 5\,°C$ (test 1/1 = 4.04%, test 1/2 = 3.39%). In test 1/1, the PEMFC's heaters were not turned on. Therefore, the curve corresponding to this test shows a lower efficiency for the system, with no significant rise of efficiency for the duration of the experiment. Test 1/2 reached a zero power output around 240 s. When compared to Figure 7a, it is seen that at this point, the PEMFC's temperature dropped below 5 °C. At this point, the PEMFC is switched off by the control strategy.

After conducting these four tests, further testing revealed a considerable drop in power output of the PEMFC for the same testing parameters.

4. Discussion

The following section discusses the proposed heating control strategies in order to reliably operate a portable FC system in subfreezing temperatures. First, the effect to the required energy is discussed. Then, the influence of the control strategies on efficiency and reliability is analyzed.

4.1. Required Energy and Thermal Behaviour

The variables measured in the experiments show the behavior that was expected from the simulative investigation. In addition, the experimental investigation allowed for the efficiency and reliability to be taken into account. The amount of power required by the heaters in all four tests was around 100 W (divided into approx. 30 W for the hydrogen tank's heater and 70 W for the PEMFC heater). This can be delivered by commercially available energy buffers, which are required in such a system as buffer storage between the PEMFC and the motor electronics. The ambient temperature T_a does influence the amount of time the heater is turned on. However, the temperature T_a does have an impact on the required energy for the heaters. More heating energy is saved if the system is set at higher temperatures, and the heating strategies shut down the heaters at lower temperatures. This behavior was also shown by Oszcipok et al. Here, the amount of energy required for heating the PEMFC is highly dependent on the ambient temperature T_a due to the heat transfer between the prototype and its surroundings [14].

When looking at the required heating energy for the tests, there are deviations between the simulations and the experiments. However, the qualitative progression between simulation and experiment matches all four tests. Both investigations showed that the energy consumption is higher when both heaters are turned on. This behavior can be seen in Figures 6 and 7b, where the three different slopes for the curve can be observed. The steepest slope corresponds to the case where both heaters were turned on. Next, the second steepest slope corresponds to the case where only the hydrogen tank's heater was on. Finally, the flattest the three curves (ca. 0%) corresponds to the test where both heaters were turned off.

Test 1/1 showed the smallest deviation between simulation and experiment, calculated with the relative model error, for the start-up time. This test had the smallest start-up time with a positive relative model error. The relative model error of the required start-up heating energy is smallest in test 1/2. The relative model error for the start-up time is negative in test 1/1 and larger in its absolute value compared to test 1/1. Test 2/2 had the longest start-up time and showed the largest absolute relative model error for the required heating energy. Both model errors were negative in this test. Therefore, in the four tests, the absolute relative model error for the heating energy increased with an increasing start-up time. The relative model error turned with increasing starting time from positive to negative. This indicates that the heating losses were underestimated in the simulation. The heat coefficients and heat flows were assumed too low. The error adds up in the transmitted energy with increasing time. This leads to an underestimation of the required heating energy in the simulation. With an increasing start-up time, this leads to an increasing negative relative model error. The underestimated heating losses does not have a large effect in test 1/1 due to the small temperature difference between T_a and T_{HO}, therefore resulting in a small start-up time. With the larger temperature difference in the three other

tests, the effect of this error increases and leads to a negative relative model error. As the relative model error for the heating energy in test 1/1 is quite small at 16.5%, it can be assumed that the thermal masses were modelled in the right range. The experimental determination of heat transfer coefficients would reduce the error in the simulations and make the results more valid.

With the simulations, an energy buffer can be selected to carry out the heating strategies at an early development stage to enable frontloading. Furthermore, with the experiments, it can be determined if this energy buffer is sufficient for the device to function accordingly. The results shown in Figure 7a indicate that for the worst-case scenario (i.e., test 2/2: subfreezing start-up and heating strategy up to the PEMFC's nominal operating temperature), the amount of energy required from the energy buffer is ca. 24 kJ. This amount of energy can be provided by the energy buffer storage used in the prototype, which has a capacity of 43.3 kJ.

The ambient temperature T_a has an impact on the required heating energy in the control strategy. The temperature at which the heaters are turned off, T_{HO}, which is directly implemented in the control strategy, had a higher impact on the required energy, as seen in Figure 7b, than the ambient temperature T_a. This shows that portable fuel cell power systems are in principle capable of starting in subfreezing conditions. This also shows that the control strategy can have a higher impact on the energy requirements, and therefore on the design of the electrical system, compared to that of the ambient temperature.

The simulations carried out applied a handful of simplifications to the model. Notably, simplifications in the heat coefficient caused deviations in the results and are the main limitation for the simulations. Nevertheless, the tendencies presented by the simulation and tests are qualitative similar. As a result, this simulation model can be considered to assess how the system would behave in practice. With these simulations, it was possible to approximate how the PEMFC system would behave under different ambient temperatures and under different parameters for the heating strategies.

4.2. Influence of the Control Strategies on Efficiency and Reliability

As Datta et al. showed, the voltage and power output is lower for lower temperatures of the PEMFC. They also showed that the PEMFC's voltage is at 50% of its rated voltage when it is operated at 10 °C [19]. This phenomenon can be seen when looking at the efficiency of the fuel cell, which is highly dependent on its power output. The tests confirm this, as the results show that using a larger amount of heating energy during a cold start-up leads to the higher efficiency of the fuel cell system. However, since more energy is needed for heating, this reduces the overall efficiency in addition. For an optimal control strategy, the heating energy and the efficiency must be taken into account, which are in conflict with each other.

This is seen in Figure 8b, as test 2/1 and test 2/2 reached a higher efficiency but also required a higher amount of energy. This is indicated in Figure 7a. Another aspect is the tendency of the fuel cell's temperature to stabilize itself after the heater has been turned off. This shows that after reaching a sufficiently high temperature, the fuel cell's operation can produce enough heat to keep the device running even under a subfreezing ambient temperature T_a. This phenomenon was also shown by Oszcipok et al. [14]. This shows that using less heating energy for the fuel cell system could be sufficient for a reliable cold start-up. However, this is only the case if the ambient temperature T_a is not too low, as this does not necessarily lead to better results. When comparing the temperature development over time between test 1/1 and test 1/2, it is seen that for ambient temperatures T_a above 0 °C, the device is capable of heating itself. With this, it avoids damaging its membrane, and as a result, the heating strategies are not required to assure the reliability of the system under these conditions.

If the ambient temperature T_a is too low or lies below 0 °C, it cannot heat itself up fast enough to avoid damage to the membrane. This is due to the fact its temperature would drop below the freezing point of water. If it is too cold, and the fuel cell is not sufficiently

heated, the heat exchange with the environment can cause the heating strategy to shut down the fuel cell to prevent permanent damages in the membrane. This happens due to the temperature dropping to values too close to or below the freezing point of water (see Figure 7a). Therefore, the goal of reducing the required heating energy is in conflict with optimizing the PEMFC's output.

The phenomenon shown by Cho et al. and by Datta et al. demonstrated how the fuel cell suffers an irreversible performance decay during a subfreezing start-up. On the other hand, Chiang et al. showed that the power output of a fuel cell is reduced for lower temperatures. Both of these phenomena could be reduced and/or totally avoided [12,13,19]. The results of this study could also help patents such as those proposed by Thompson et al. or Jang et al. by allowing these to be applied to a wider range of portable applications [40,41].

If the temperature of the fuel cell drops far enough, this would cause the water inside the cathode to begin to freeze. In turn, this would lead to an irreversible performance decay of the cell. Therefore, the heating strategies are vital for the reliable operation of the fuel cell under ambient temperatures T_a below 0 °C. For subfreezing temperatures, a more reliable control strategy is required, as supplying too little heating energy may cause permanent damage to the fuel cell. For ambient temperatures T_a above 0 °C, a more experimental control strategy to save heating energy can be implemented. For these reasons, the appropriate selection of a heating strategy for the cold start-up of a fuel cell system can significantly influence its efficiency and reliability. Due to reliability reasons, a differentiation in the control strategy between subfreezing and non-subfreezing through the heater shut off temperature is recommended.

5. Conclusions

The influence of the heating strategies during a cold start-up on a portable PEMFC system were investigated experimentally and through simulations. The necessary energy supply required to establish the efficiency and reliability of the fuel cell system were investigated.

To start, for a fuel cell system at an ambient temperature T_a of −3 °C, an energy buffer would have to deliver 25 kJ of energy to the heaters. Notably, this value can be obtained from traditional batteries. This energy buffer is strongly dependent on the control strategy, which is specified by the temperature at which the heater is turned off. It should be noted that the energy buffer impacts the efficiency of the fuel cell system. The ambient temperature, however, has a smaller impact on the required energy than the temperature at which the heater is turned off. The ambient temperature T_a impacts how fast the fuel cell will cool down after the heaters are shut off. The results also revealed that heating the fuel cell above 5 °C leads to a higher power output and efficiency of the fuel cell system.

When a higher efficiency of the fuel cell system is required, a greater energy supply is needed for the heating strategies. Using less heating energy (i.e., heating the PEMFC to a lower temperature) can save energy, but it may impact the reliable operation of the PEMFC system. It is proposed to adjust the control strategy regarding the ambient temperature whether it is subfreezing or non-subfreezing. For subfreezing ambient temperatures, a more reliable control strategy is required. This is to ensure its reliability, as subfreezing temperatures can cause permanent damage to the fuel cell membrane.

These findings help in dimensioning the energy buffer. The heat transfer coefficients are an uncertainty in the simulative design of such a system at an early development stage and should be validated with extra experiments. A miscalculation of the heat transfer coefficients can harm the reliability although a subfreezing start-up would be possible. Sufficient energy must be considered for the portable device to perform its function. The fuel cell loads the energy buffer in operation. Enough charge must be left in the energy buffer to heat up the fuel cell system the next time it is used. Therefore, the fuel cell can only switch off when this critical amount of energy is available in the energy buffer.

The findings with respect to the heating strategies help to improve reliability and efficiency during operation of a portable fuel cell system. Subfreezing temperatures were

identified as a critical factor of the control strategy. Therefore, the distinction between subfreezing and non-subfreezing ambient temperatures has to be considered in the control strategy to ensure its reliability.

References

1. Dicks, A.L.; Rand, D.A.J. *Fuel Cell Systems Explained*; Wiley: London, UK, 2018; ISBN 9781118613528.
2. Fraunhofer-Institut für Keramische Technologien und Systeme IKTS. LTCC-PEMFC. Available online: https://www.ikts. fraunhofer.de/content/dam/ikts/abteilungen/elektronik_mikrosystemtechnik/Hybride_Mikrosysteme/IKTS_Ltcc-pemfc. pdf (accessed on 1 March 2022).
3. Ballard Power Systems, Inc. FCveloCity-HD: Fuel Cell Power Module for Heavy Duty Motive Applications. Available online: https://www.ballard.com/docs/default-source/spec-sheets/fcvelocity-hd.pdf?sfvrsn=2debc380_4 (accessed on 23 August 2021).
4. Kaya, K.; Hames, Y. (Eds.) A study on fuel cell electric unmanned aerial vehicle. In Proceedings of the 4th International Conference on Power Electronics and their Applications, Elazig, Turkey, 25–27 September 2019.
5. Krcum, M.; Gudelj, A.; Juric, Z. (Eds.) Fuel cells for marine application. In Proceedings of the 46th International Symposium Electronics in Marine, Zadar, Croatia, 18 June 2004.
6. Weydanz, W. (Ed.) *Power Tools: Batteries*; Elsevier: Amsterdam, The Netherlands, 2009; ISBN 978-0-444-52093-7.
7. Julien, C.; Mauger, A.; Vijh, A.; Zaghib, K. *Lithium Batteries*; Springer International Publishing: Cham, Switzerland, 2016; ISBN 978-3-319-19107-2.
8. Wilberforce, T.; Alaswad, A.; Palumbo, A.; Dassisti, M.; Olabi, A.G. Advances in stationary and portable fuel cell applications. *Int. J. Hydrogen Energy* **2016**, *41*, 16509–16522. [CrossRef]
9. Kyoung, S.; Ferekh, S.; Gwak, G.; Jo, A.; Ju, H. Three-dimensional modeling and simulation of hydrogen desorption in metal hydride hydrogen storage vessels. *Int. J. Hydrogen Energy* **2015**, *40*, 14322–14330. [CrossRef]
10. Al-Baghdadi, M.A.R.S.; Al-Janabi, H.A.K.S. Numerical analysis of a proton exchange membrane fuel cell. Part 1: Model development. *Proc. Inst. Mech. Eng. Part A J. Power Energy* **2007**, *221*, 917–929. [CrossRef]
11. Kazim, A.; Lund, P. Basic parametric study of a proton exchange membrane fuel cell. *Proc. Inst. Mech. Eng. Part A J. Power Energy* **2006**, *220*, 847–853. [CrossRef]
12. Cho, E.; Ko, J.-J.; Ha, H.Y.; Hong, S.-A.; Lee, K.-Y.; Lim, T.-W.; Oh, I.-H. Effects of Water Removal on the Performance Degradation of PEMFCs Repetitively Brought to <0 °C. *J. Electrochem. Soc.* **2004**, *151*, A661. [CrossRef]
13. Chiang, M.-S.; Chu, H.-S. Effects of Temperature and Humidification Levels on the Performance of a Proton Exchange Membrane Fuel Cell. *Proc. Inst. Mech. Eng. Part A J. Power Energy* **2006**, *220*, 435–448. [CrossRef]
14. Oszcipok, M.; Zedda, M.; Hesselmann, J.; Huppmann, M.; Wodrich, M.; Junghardt, M.; Hebling, C. Portable proton exchange membrane fuel-cell systems for outdoor applications. *J. Power Sources* **2006**, *157*, 666–673. [CrossRef]
15. Amamou, A.A.; Kelouwani, S.; Boulon, L.; Agbossou, K. A Comprehensive Review of Solutions and Strategies for Cold Start of Automotive Proton Exchange Membrane Fuel Cells. *IEEE Access* **2016**, *4*, 4989–5002. [CrossRef]
16. Fuller, T.F.; Wheeler, D.J. Start up of Cold Fuel Cell. Patent 17733198, 22 October 1998.
17. Fuss, R.L.; Thompson, E.L. Control System and Method for Starting a Frozen Fuel Cell. U.S. Patent 22237702, 16 August 2002.
18. Min, K.Y.; Jun, K.J.; Uk, K.S.; Hyun, L.J.; Woo, L.N.; Jae, S.I.; Suk, S.W. Purge System for Fuel Cell with Improved Cold Start Performance. U.S. Patent 87231310, 31 August 2010.
19. Datta, B.K.; Velayutham, G.; Goud, A.P. Fuel cell power source for a cold region. *J. Power Sources* **2002**, *106*, 370–376. [CrossRef]
20. Pistono, A.O.; Rice, C.A. Subzero water distribution in proton exchange membrane fuel cells: Effects of preconditioning method. *Int. J. Hydrogen Energy* **2019**, *44*, 22098–22109. [CrossRef]

21. Hobmeyr, R.T.J.; Wexel, D.M. Cold Start Pre-Heater for a Fuel Cell System. U.S. Patent 7368196B2, 3 February 2004.
22. Clingerman, B.J.; Kirklin, M.C.; Rainville, J.D. Cold Start Compressor Control and Mechanization in a Fuel Cell System. U.S. Patent 68490607, 12 March 2007.
23. Limbeck, U. Method to Cold-Start Fuel Cell System at Sub-Zero Temperatures. U.S. Patent 58864505, 4 February 2005.
24. Lin, B. Thermal Control of Fuel Cell for Improved Cold Start. U.S. Patent 2006024378, 21 June 2006.
25. Limbeck, U. Cold Start Facility for Fuel Cells at below Zero Temperatures Has Heated Fluid Circulated through Cell. Patent 102004005935, 6 February 2004.
26. Travassos, M.A.; Lopes, V.V.; Silva, R.A.; Novais, A.Q.; Rangel, C.M. Assessing cell polarity reversal degradation phenomena in PEM fuel cells by electrochemical impedance spectroscopy. *Int. J. Hydrogen Energy* **2013**, *38*, 7684–7696. [CrossRef]
27. Luo, L.; Huang, B.; Cheng, Z.; Jian, Q. Rapid degradation characteristics of an air-cooled PEMFC stack. *Int. J. Energy Res.* **2020**, *44*, 4784–4799. [CrossRef]
28. Plant, L.B.; Rock, J.A. Method of Cold Start-Up of a PEM Fuel Cell. Patent EP00124165, 7 November 2000.
29. Nobuo, F.; Kimihide, H.; Kenji, K.; Tadaichi, M.; Hiroaki, M.; Shinya, S.; Naohiro, Y. Fuel Cell System and Method of Starting the Frozen Fuel Cell System. U.S. Patent 20060141309A1, 20 November.
30. Iwasaki, Y.; Wakabayashi, K. Freeze Protected Fuel Cell System. Patent 03014169, 24 June 2003.
31. Scott, D. FCPM Freeze Start Heater. U.S. Patent 86471604, 9 June 2004.
32. Docter, A.; Frank, G.; Konrad, G.; Lamm, A.; Mueller, J.T. Fuel Cell and Method of Cold Start-up of Such a Fuel Cell. Patent 03004709, 4 March 2003.
33. Zimprich, S.; Matthiesen, S.; Gwosch, T. Hydrogen as Energy Supply for Mobile Applications Using the Example of a Power Tool. *Konstruktion* **2022**, 65–69. [CrossRef]
34. Barroso, J.; Renau, J.; Lozano, A.; Miralles, J.; Martín, J.; Sánchez, F.; Barreras, F. Experimental determination of the heat transfer coefficient for the optimal design of the cooling system of a PEM fuel cell placed inside the fuselage of an UAV. *Appl. Therm. Eng.* **2015**, *89*, 1–10. [CrossRef]
35. Njoya, S.M.; Tremblay, O.; Dessaint, L.-A. A generic fuel cell model for the simulation of fuel cell vehicles. In Proceedings of the 2009 IEEE Vehicle Power and Propulsion Conference (VPPC), Dearborn, MI, USA, 7–10 September 2009; pp. 1722–1729.
36. Horizon Fuel Cell Technologies. H-20 Fuel Cell Stack: User Manual. Available online: https://2fca7bd6-9a97-4678-bc9f-28d3354f6ea2.filesusr.com/ugd/047f54_17ecd01808c4ffa1b478d67ed1e45470.pdf (accessed on 19 August 2021).
37. Schroder, T.; Gwosch, T.; Matthiesen, S. Comparison of Parameterization Methods for Real-Time Battery Simulation Used in Mechatronic Powertrain Test Benches. *IEEE Access* **2020**, *8*, 87517–87528. [CrossRef]
38. Huber Kältemaschinenbau AG. Huber Unistat 425 with Pilot ONE. Available online: https://www.huber-online.com/en/product_datasheet.aspx?no=1050.0010.01 (accessed on 1 March 2022).
39. Jäger Computergesteuerte Messtechnik GmbH. ADwin-Pro II: System and Hardware Description. 2018. Available online: https://smt.at/wp-content/uploads/adwin-pro-ii-system-and-hardware-description.pdf (accessed on 1 March 2022).
40. Fuss, R.L.; Thompson, E.L. Combustion-Thawed Fuel Cell. Patent 11212905, 22 April 2005.
41. Sang, J.K.; Han, K.J. End Cell Heater for Fuel Cell. U.S. Patent 20210007185, 14 July 2017.